Research

Author for correspondence:
Fritz-Olaf Lehmann
e-mail: fritz.lehmann@uni-rostock.de

# Proprioceptive feedback determines visuomotor gain in *Drosophila*

Jan Bartussek and Fritz-Olaf Lehmann

Department of Animal Physiology, Institute of Biological Sciences,
University of Rostock, Albert-Einstein-Straße 3, Rostock 18059, Germany

Multisensory integration is a prerequisite for effective locomotor control in most animals. Especially, the impressive aerial performance of insects relies on rapid and precise integration of multiple sensory modalities that provide feedback on different time scales. In flies, continuous visual signalling from the compound eyes is fused with phasic proprioceptive feedback to ensure precise neural activation of wing steering muscles (WSM) within narrow temporal phase bands of the stroke cycle. This phase-locked activation relies on mechanoreceptors distributed over wings and gyroscopic halteres. Here we investigate visual steering performance of tethered flying fruit flies with reduced haltere and wing feedback signalling. Using a flight simulator, we evaluated visual object fixation behaviour, optomotor altitude control and saccadic escape reflexes. The behavioural assays show an antagonistic effect of wing and haltere signalling on visuomotor gain during flight. Compared with controls, suppression of haltere feedback attenuates while suppression of wing feedback enhances the animal's wing steering range. Our results suggest that the generation of motor commands owing to visual perception is dynamically controlled by proprioception. We outline a potential physiological mechanism based on the biomechanical properties of WSM and sensory integration processes at the level of motoneurons. Collectively, the findings contribute to our general understanding how moving animals integrate sensory information with dynamically changing temporal structure.

1. Introduction

Rapid and precise integration of multiple sensory modalities is essential for efficient control of locomotion [1]. This is especially apparent in flies performing escape manoeuvres, during which the animal generates fast, directed turns away from an approaching predator and actively re-stabilizes body posture within milliseconds [2–4]. This remarkable manoeuvre exemplifies the integration of feedback signals from two highly
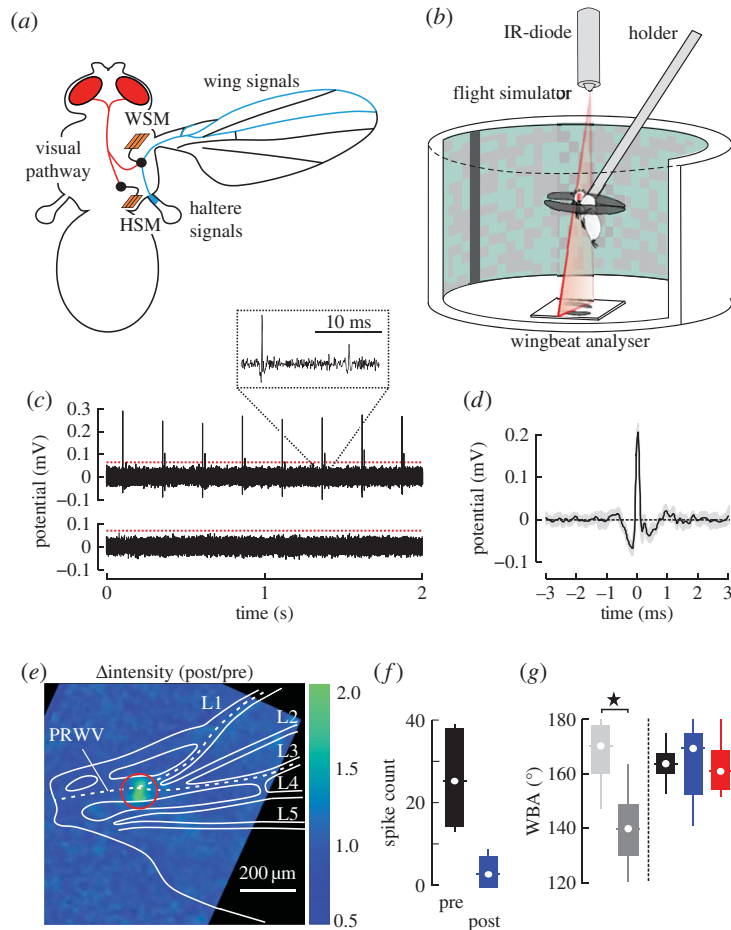
Figure 1. Experimental approach. (*a*) Schematic of sensory pathways in flies. The visual system (red) projects to the haltere (HSM) and wing steering muscles (WSM). Mechanosensory afferents (blue) from campaniform sensillae on halteres and the wings connect to motoneurons of the WSM (black). (*b*) Experimental set-up. Individual flies are tethered to a holder and flown in a virtual-reality flight simulator in which wing kinematics are measured using a wingbeat analyser. (*c*) Neural activity of wing nerve (black) during mechanical stimulation of campaniform sensillae (4 Hz stimulus frequency). Top trace, before laser application; bottom trace, after laser application (35 mW). Spike initiation is detected by a software algorithm. Red line indicates threshold value. (*d*) Averaged spiking response during mechanical stimulation (single wing, $N = 8$ spikes). Grey area shows standard deviation. (*e*) Relative change in fluorescence intensity (post–pre-application stimulus ratio) plotted in pseudo-colour after local (red ring) application of a 35 mW laser pulse. Wing structures are retraced from bright-field microscopy and wing nerve is shown according to anatomical studies (white, dashed line). PRWV, proximal radial wing vein. (*f*) Tukey box plots of spike counts prior to (pre) and after (post) 35 mW laser treatment of the wing nerve ($N = 6$ wings). (*g*) Tukey box plots of mean wingbeat amplitude during optomotor lift stimulation. Amplitude of non-treated (light grey) and 90 mW-treated wings (dark grey) are scored in animals in which we heat-treated only a single wing. For comparison, data from intact (black, $N = 25$ flies), bilaterally wing nerve treated (blue, 35 mW, $N = 9$ flies) and bilaterally haltere-immobilized animals (red, $N = 22$ flies) are shown on the right. Data were derived from approximately 4200 wing strokes of each fly. $^*p < 0.05$.

evolved sensory systems, the visual system and the halteres: the visual system computes the optic flow of the environment [5], detects the approaching predator such as a dragonfly and initiates the saccadic escape response, which is eventually terminated by signals provided by the two halteres [6,7] (figure 1*a*).

Halteres are small, club-shaped organs that beat in anti-phase with the wings but apparently have no aerodynamic function. Instead, the halteres serve as a gyroscopic sensor that elicits compensatory wing movements within one or two wing strokes [8–12]. The haltere base is covered with fields of mechanoreceptors, possessing fast, monosynaptic connections to motoneurons of wing steering muscles (WSM) [13–16]. Some of these fields are activated in every wing stroke, providing timing cues for the motor system [17,18]. During body turns, rotational forces bend the halteres out of their normal beating plane [17,19]. Depending on strength and direction of these alterations, activation phase of the mechanoreceptors changes with respect to the wing flapping phase, generating body motion-dependent phase-locked feedback signals within each stroke cycle [20,21]. Neural projections from halteres to

WSM are supplemented by projections from mechanoreceptors located on the insect wings [13,16,22]. A recent study has shown their significance for body posture control in moths [23]. In flies, wing mechanoreceptors probably contribute to the timing of WSM activation [18,24,25], providing feedback on wing loading [26] and wing deformation caused by the travel of torsional waves over the wing surface [27]. The functional role of wing mechanoreceptors for flight control, however, is not well understood [28].

A critical, unanswered question is how the 'slow' (approx. 30 ms delay) feedback from the compound eyes is fused with the 'fast' (approx. 3–5 ms delay) wingbeat-synchronous mechanosensory signalling. This integration process is a prerequisite to ensure phase-locked WSM activation during visual steering [1,15,18]. A potential mechanism of the process includes a re-routing of visual input via the haltere feedback circuitry [29] (figure 1*a*). Halteres possess their own set of steering muscles that is under direct visual control, while electrophysiological evidence for direct visual input to the WSM is missing [30]. Hence, vision might indirectly influence WSM spike timing by manipulation of haltere feedback generation. This re-routing hypothesis, however, has not yet been confirmed in a behavioural assay. On the contrary, results question the significance of visual re-routing for flight control. Sherman & Dickinson [31] showed that during concurrent and conflicting visual and mechanical stimulation, visual feedback does not change the response to mechanical stimuli. This cannot easily be explained in the context of the re-routing hypothesis. Exclusive visual re-routing even predicts that flies with a loss in haltere function face a total loss of vision-induced flight behaviours. Mureli & Fox [32], however, recently showed that tethered flies with disabled halteres are still capable of vision-guided flight control.

In this study, we investigated the significance of both wing and haltere feedback on vision-guided flight in the fruit fly *Drosophila melanogaster*. We attenuate feedback from halteres by mechanically disabling haltere movement and feedback from wings by ablating the wing nerve with an infrared laser (figure 1*c–g*). As flies with immobilized halteres are not capable of flying freely, owing to the loss of gyroscopic feedback, we tested the animals in a flight simulator under tethered flight conditions (figure 1*b*). We scored the animals according to their vision-guided steering performance employing three prominent and robust behavioural assays: object fixation behaviour, optomotor altitude control, and saccadic escape reflexes. Our results show an antagonistic effect of haltere and wing mechanosensory feedback on wing kinematics, suggesting that visuomotor gain in flies is determined by proprioceptive feedback.

2. Material and methods

2.1. Animals and tethering

All experiments were conducted with 4- to 5-day-old female Canton S wild-type *D. melanogaster* obtained from our laboratory stock. The flies were reared on commercial *Drosophila* medium (Vos instrumenten, The Netherlands) and kept under a 12 L : 12 D cycle at 24°C ambient temperature. The animals were manipulated under cold-anaesthesia using a Peltier stage at approximately 4°C. After manipulation of wings and halteres, we glued the head of the flies to the thorax and tethered the animals between the head and the notum to a 7.3 mm long, 0.13 mm diameter tungsten rod using UV-light activated glue (Clear Glass Adhesive, Henkel Loctite, Germany). After tethering, the animals were allowed to rest for at least 60 min before we placed them into the flight simulator.

2.2. Feedback suppression

Previous research showed that the haltere's sensory sensillae are inactivated in immobilized halteres [11,33]. We thus disabled haltere motion by applying a small droplet of UV-light-activated glue near the haltere base. Curing time was approximately 20 s using a 150 W Osram halogen lamp. To abolish feedback from campaniform sensillae of both wings, we heat-shocked the proximal radial wing vein that contains the wing nerve [34] (figure 1*a,e*). The animal was positioned under a dissecting microscope with its ventral side pointing up and wings pulled sideways. A trigger-controlled near infrared diode laser (Lasiris DLSC 830 nm, Coherent, USA) was aligned with the optical pathway of the microscope using a dichroic, infrared mirror (IR Mirror 46386, Edmund Optics, USA), allowing precise visual adjustment of the laser beam on the wing vein. We calibrated the laser light using a low power thermopile (XLP12-3S-H2-INT, Laser Components, Germany), which yielded approximately 143 mW maximum output power at maximum supply voltage. The diameter of the circular laser spot on the wing was approximately 130 µm.

To avoid mechanical damage of the vein's cuticle while providing enough heat to severely attenuate signal transmission of the wing nerve, we conducted a series of control experiments. We first estimated the dependency between visible cuticle damage and the power of a single laser pulse while keeping the pulse duration fixed at 0.55 s. We found that a 90 mW pulse is sufficient for perforation of the wing vein, while pulses exceeding 70 mW only caused darkening of the cuticle. Below this threshold, we found no sign of mechanical wing damage. Based on these results, we used a pulse power of 50% the threshold value (35 mW). Total power of a single 35 mW laser pulse after reflection by the dichroic mirror was approximately 18 mJ. For comparison, Sinha *et al.* [35] used a train of approximately hundred UV laser pulses (193 nm) with an energy of 170 µJ each (approx. 17 mJ total energy) in order to perforate the head cuticle in *Drosophila* for functional brain imaging. Considering approximately 4.3 times smaller photon energy and approximately 10 times larger cuticle transmission at 830 nm compared with 193 nm wavelength [36], total thermal energy applied to the wing cuticle is only approximately 2.3% of the critical value suggested by Sinha *et al.* [35]. The risk of heat-induced cuticle weakening was thus negligibly small (see also section below).

2.3. Controls

We evaluated the impact of heat treatment on neural transmission inside the wing nerve employing both fluorescence imaging and electrophysiological recordings. Fluorescence imaging of the wing nerve in transgene animals, genetically encoding the calcium-sensitive fluorescence protein Cameleon 2.1, showed a strong increase in local fluorescence ($284 \pm 73\%$, $p = 0.007$, $N = 10$ wings, figure 1*e*) following laser pulse application. A similar increase in calcium-dependent fluorescence has been observed during laser-induced cell death in human epithelial cells [37].

We also determined signal transmission by adapting an electrophysiological stimulation-recording technique developed for wing campaniform sensilliae in *Calliphora* [27]. A single wing was slightly cut at both ends and positioned between two copper electrodes connected to an amplifier (ISO80, World Precision Instruments, USA) and a data acquisition system (USB-6009, National Instruments, USA). Ringer solution established electrical contact. To mechanically stimulate the sensillae, a stiff bristle on a wooden rod was glued to a loudspeaker. A signal generator generated sinusoidal 13 Hz movements during which the bristle cyclically tapped on the wing at approximately half wing length. We stimulated the wing prior to heat treatment for approximately 5 s, subsequently applied a single laser pulse and repeated the recording ($N = 6$ wings). Wing nerve spikes were detected using a self-written software algorithm with a detection threshold of four times standard deviation of the recorded data (figure 1*c*,*d*). On average, we counted 25.5 ± 4.6 spikes prior to and 3.2 ± 1.5 spikes after laser pulse application (means $\pm$ s.d., $p = 0.01$, $N = 6$, figure 1*f*), demonstrating the pronounced effect of heat on the generation of neural feedback.

Moreover, to exclude that laser treatment leads to an unwanted mechanical damage that alters wing motion, we scored wingbeat amplitude (WBA) of tethered animals flying in a flight simulator during open-loop altitude stimulation. We compared untreated intact controls with flies that experienced 35 mW or 90 mW laser treatment. In flies in which one wing was treated with a single 90 mW laser pulse, mean amplitude is significantly smaller in the treated wing (approx. $138 \pm 1.7°$, $p < 0.001$, $N = 9$, dark grey, figure 1*g*) but similar in the non-treated wing (approx. $163 \pm 4.9°$, $p = 0.30$, light grey, figure 1*g*), compared with controls (mean of both wings, approximately $165 \pm 1.8°$, $N = 25$, black, figure 1*g*). In this particular case, the amplitude median of the non-treated wing in 90 mW-treated flies (approx. $169 \pm 22.7°$ interquartile range) is slightly higher than that of controls (approx. $164 \pm 6.4°$ interquartile range, figure 1*g*). A possible explanation for this weak trend might be an imbalance in left–right flight muscle mechanical power distribution owing to a reduction in power requirements for flight during low-amplitude wing flapping. Consistent with the above findings, the top 1% minimum (approx. $123 \pm 6.2°$) and maximum amplitudes (approx. $160 \pm 6.2°$) of the 90 mW-treated wing are significantly smaller than those in controls (approx. $149 \pm 1.9°$ and approx. $176 \pm 1.7°$, $p < 0.001$, $N = 25$), respectively. Mean WBA of 35 mW-treated wings (approx. $167 \pm 4.2°$, $N = 9$), by contrast, is not significantly different from the mean in intact flies ($p = 0.30$, see the electronic supplementary material, figure S1, for raw data traces). Altogether, we conclude that there is no significant mechanically induced change in wing motion at 35 mW heat treatment.

In flies, haltere motion is mechanically coupled with wing motion via the thoracic exoskeleton, which might cause mechanical cross-talk between halteres and wings [38]. To estimate this potential cross-talk, we calculated the maximum power (peak inertia) that the two moving halteres might transfer to the wings during flight. We derived the haltere's centre of mass (CoM) from an elementary blade approach

[16] and haltere kinematics from the velocity profile of haltere movement, measured in the blowfly [19]. The distance between CoM and haltere hinge is approximately 215 μm, total mass of both halteres is approximately 0.8 μg [12] and wingbeat frequency (WBF) is 200 Hz. Data show that total inertial peak force of both halteres equals approximately 0.6 μN. This is approximately 5% of total flight force required to support body mass (approx. 13 μN) in *D. melanogaster* [39], rendering a mechanical effect of haltere immobilization on wing motion unlikely.

## 2.4. Experimental set-up and visual stimulation

The animals were flown in a virtual-reality flight simulator (figure 1*b*) that has previously been described [39]. The simulator consists of a circular array of green, light emitting diodes with an effective spatial resolution of 0.2°. An infrared diode above the simulator casts shadows of the wings on an infrared sensitive photo-diode connected to a custom-built electronic wingbeat analyser, providing voltage equivalents of WBA and frequency. We converted the measures into angular degrees using video images recorded by an infrared-sensitive camera and using custom-written software routines (Origin, Originlab Corporation, USA). The visual panorama displayed in the simulator was updated every 8 ms (12 ms in the case of the escape response assay) and data sampling frequency was 125 Hz.

For visual stimulation, we used a 12° wide, vertical black stripe as foreground and various background patterns for three behavioural assays: a random dot pattern (object fixation behaviour), a horizontal stripe grating (optomotor altitude control), and a visually expanding visual object (saccadic escape reflexes). The random dot background consisted of 2205 bright and dark, 8° wide square image pixels, the grating was composed of four horizontal grey stripes, and the expanding object was a black dot (figures 1*b* and 2). The Michelson contrast between bright and dark image pixels was approximately 0.21 (random dot pattern, horizontal stripes) and approximately 0.89 (expanding object), and approximately 0.87 between the black stripe and mean background brightness. The foreground was under closed-loop feedback control in all experiments, allowing the animal to actively control azimuth velocity and thus position of the visual object by changing the relative difference between its left and right WBA (left minus right). This measure is proportional to yaw moment around the vertical body axis [40]. During object fixation, we continuously provided the animal with a steering task by adding a sinusoidal, 0.5 Hz velocity bias to the stripe feedback signal (150° s^{-1} oscillation amplitude).

To simulate free flight conditions in which the visual foreground object moves in front of the background, the random dot pattern was controlled by the inverted feedback signal. This caused relative motion between both patterns [41]. The horizontal grating background oscillated sinusoidally up and down in open loop (50° s^{-1} oscillation amplitude and 0.5 Hz frequency). Saccadic manoeuvres in the escape response assay were triggered by the black dot background that rapidly expanded every 5 s in the fly's lateral field of view with approximately 813° s^{-1} from 18° to 96° angular size. The expanded object was displayed for 892 ms before it vanished from the screen of the simulator.

2.5. Simulated damping coefficient

Flight control in insects depends not only on several factors including feedback from sensory organs but also on the animal's physical properties such as body mass moments of inertia and frictional damping (for a review, see [42]). In the present experiments, we thus calculated the instantaneous angular velocity of the visual pattern from the animal's instantaneous yaw moment, the mass moments of inertia and the combined frictional damping coefficient of body and wings [41]. As flight heading stability strongly depends on the ratio between moments of inertia and frictional damping, a change in damping coefficient alters the difficulty level for heading control [41]. At small damping, stripe stabilization in the fly's frontal field of view requires high precision of neuromuscular control. In this case, coarse modulation in wing kinematics increases the risk of oversteering and thus a loss of stripe control. Elevated damping, by contrast, favours stable flight heading but forces the animal to produce higher yaw moments in order to stabilize the oscillating stripe [41]. To test for both fixation performance and steering range, we varied the frictional damping coefficient 20-fold. For a comparison with previously published data, we used coefficients of 52, 130, 260, 520 and 1024 pNms, where 52 pNms corresponds to the damping expected in freely flying fruit flies [41]. As visual fixation performance in tethered wild-type flies is superior at damping coefficients between 520–1024 pNms and quickly attenuates below this threshold [41], we refrained from testing damping coefficients smaller than the free flight value. During experiments in which we employed optomotor altitude stimulation and triggered escape responses, the damping coefficient was 1024 pNms.
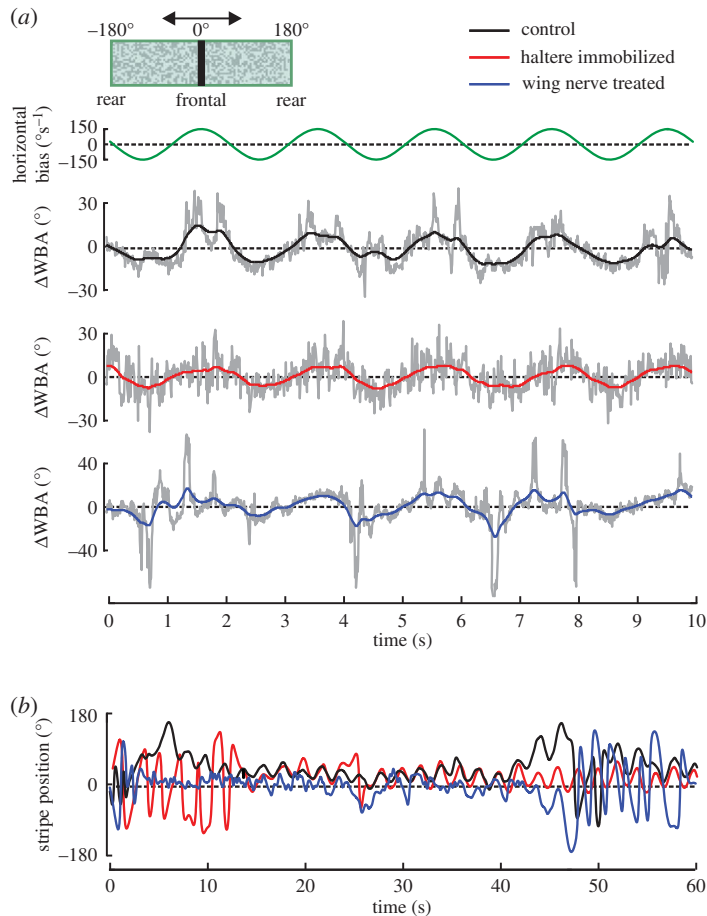
Figure 2. Typical examples of object fixation response in tethered fruit flies. (*a*) Horizontal velocity bias applied to stripe motion (top), difference between left and right wingbeat amplitude (△WBA, lower traces) and (*b*) instantaneous stripe position during object fixation in single flies. Black, intact controls; red, haltere-immobilized flies; blue, wing nerve treated flies. Grey lines show raw data, coloured traces are filtered using a first order Butterworth low pass filter with 1 Hz cut-off frequency. Aerodynamic damping coefficient was 520 pNms and inset shows visual pattern.

2.6. Data analysis and statistical methods

The data in this study were collected from 26 intact control animals, 22 animals with bilaterally disabled halteres and 14 flies with bilaterally heat-treated wing nerves. Recording time of each flight sequence was 90 s and sequences below 30 s continuous flight were excluded from the analysis. Averaged data in figures are shown as boxplots with interquartiles because data for 6 of 15 experimental conditions were not normally distributed. If not stated otherwise, values mentioned in the text are arithmetic population means ± s.e. of the mean. Means are compared using the non-parametric two-sample Kolmogorov–Smirnov test that does not require normal data distribution. Data analyses were performed using custom-written Matlab routines (MathWorks, USA).

3. Results

3.1. Object fixation behaviour

Similar to control flies (C-flies, $N = 26$), haltere-immobilized flies (HI-flies, $N = 22$) and wing nerve treated flies (WN-flies, $N = 14$) actively stabilized the azimuth position of a visual target (black stripe) under visual closed-loop feedback conditions by modulating the difference between left and right wingbeat amplitude, △WBA. To provide the animals with a continuous steering task, we added a sinusoidal velocity bias to the feedback signal controlling azimuth velocity of the black stripe (§2.4). At a mean damping coefficient of 520 pNms, most animals were capable of compensating the artificial
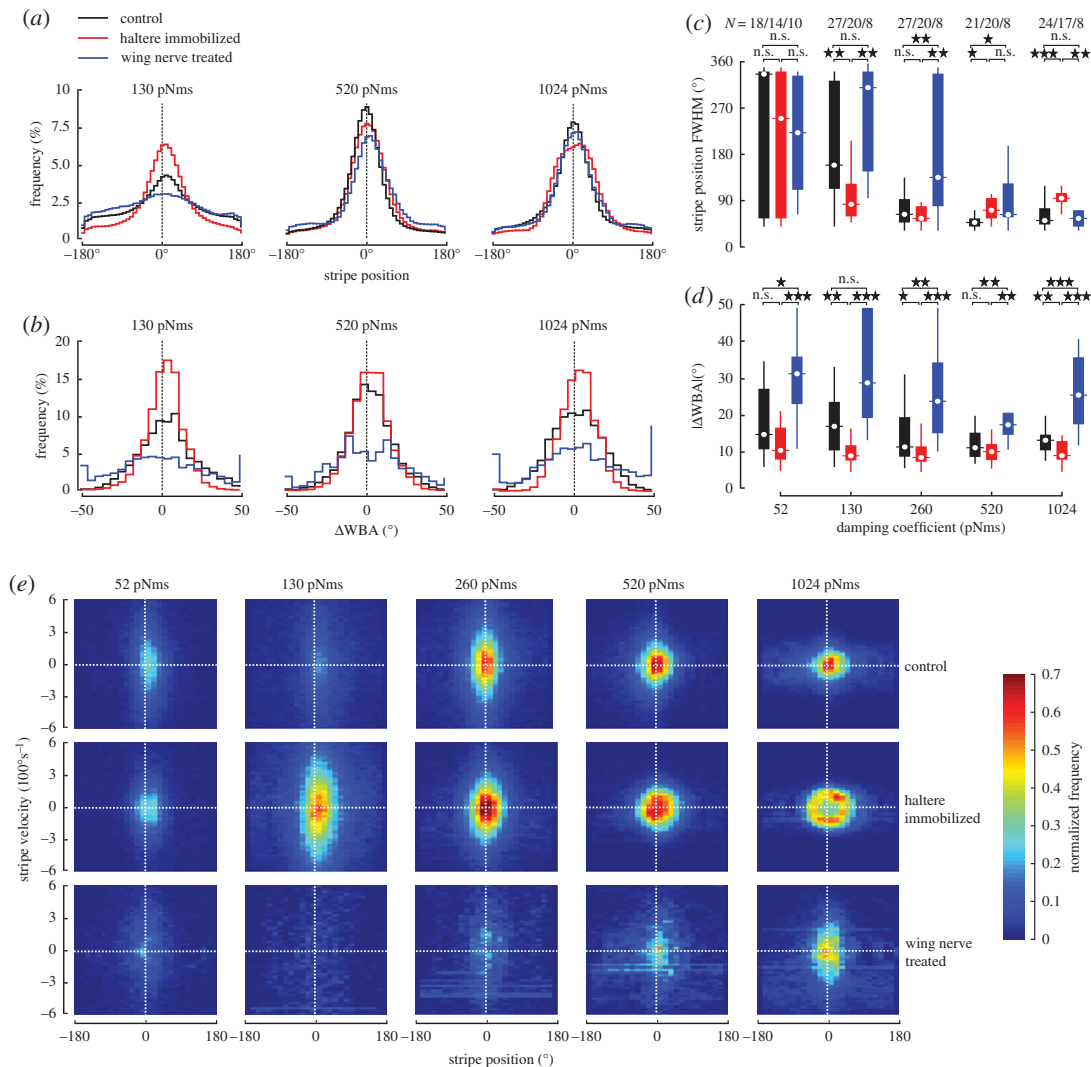
Figure 3. Statistical evaluation of object fixation response. (*a*) Normalized histograms of mean stripe position and (*b*) corresponding mean △WBA of the tested groups at three selected damping coefficients. Mean standard deviation is in (*a*) 1.27% (black), 0.96% (red) and 1.01% (blue) and in (*b*) 2.33% (black), 1.77% (red) and 4.11% (blue). ±180°, rear position; 0°, frontal position of the panorama. (*c*) Tukey box plots of half width stripe position histograms (full width at half maximum, FWHM) and (*d*) mean absolute WBA differences within a flight sequence for all tested damping coefficients. Black, intact controls; red, haltere-immobilized flies; blue, wing nerve treated flies; *N*, number of tested flies; n.s., not significant. (*e*) Phase space plots of angular velocity of the visual object (black stripe) displayed inside the flight simulator plotted against object position at five aerodynamic damping coefficients. 0° and ±180° indicate the fly's frontal and rear field of view, respectively. For each graph, we averaged 2000 flight samples each of 8–24 flies (see *c*) and sorted them into 80 velocity and 25 position bins. Normalized frequency of data points is plotted in pseudo-colour.

velocity bias and hence stabilized the displayed stripe in their frontal field of view (figure 2*a,b*). Kinematic steering range and object fixation performance, however, differ between the tested groups. The behavioural differences are evident from histograms of stripe positions and the underlying wing kinematics (figure 3*a,b*). We statistically evaluated object fixation performance of each tested group, calculating the full width at half maximum (FWHM) of each stripe position histogram and absolute WBA difference |△WBA|. We scored the animals' responses to a 20-fold change in aerodynamic damping (figure 3*c,d*) at which small damping requires precise neural control for stripe fixation and high damping elevated WBAs (§2.5). Phase space plots highlight the increase in angular velocity of the black stripe with decreasing damping, which is consistent with previous findings in fruit flies (figure 3*e*) [41].

The results obtained for C-flies are in good agreement with previously published data measured under similar conditions [41]. We found that C-flies typically steer by comparatively small changes in relative WBA and showed best stripe stabilization (60.8 ± 3.90°FWHM, *N* = 21) at 520 pNms damping,

steering with $11.9 \pm 0.73°|\Delta WBA|$. Smaller frictional damping destabilized flight, resulting in both a decrease in object fixation performance in C-flies and an up to twofold increase in $|\Delta WBA|$, owing to frequent overshoots in feedback signalling and corresponding loss in stripe control.

HI-flies displayed no gross damping-dependent change in kinematic modulation. Even the smallest $(9.2 \pm 0.68°, 260 \text{ pNms}, N = 20)$ and largest $(12.1 \pm 1.01°, 52 \text{ pNms}, N = 14)$ values for $|\Delta WBA|$ were not significantly different $(p = 0.20)$. Figure 3d further shows that HI-flies typically steered with smaller relative WBAs compared with C-flies (130, 260, 1024 pNms, $p < 0.001$), suggesting a loss in kinematic envelope of the motor control system. Surprisingly, this reduction in steering ability of HI-flies was not necessarily accompanied by a decrease in object fixation performance. At low damping of 130 and 260 pNms, FWHM of stripe position is smaller in HI-flies compared with controls (260 pNms, $p = 0.63$; 130 pNms, $p = 0.008$, figure 3c). This result cannot easily be explained by a net change in steering activity in HI-flies because the added velocity bias requires continuous kinematic responses for stripe stabilization. Under high-damping conditions, however, HI-flies performed worse than controls owing to their apparent inability to generate sufficiently large WBA differences. This prevented HI-flies from fully compensating the stripe's velocity bias (figure 3e), resulting in a 17% broader stripe position distribution (1024 pNms; FWHM: HI-flies, $110 \pm 8.6°$, $N = 17$; C-flies, $93.6 \pm 18.1°$, $N = 24$; $p < 0.001$, figure 3c).

Wing nerve treated animals, by contrast, consistently steered with elevated relative stroke amplitudes (figure 3d). These amplitudes range from $20.5 \pm 3.8°$ $(N = 8)$ at 520 pNms damping to $32.4 \pm 4.98°$ $(N = 10)$ at 52 pNms and were typically different from values determined in C-flies (52, 260, 520, 1024 pNms, $p < 0.05$; 130 pNms, $p = 0.12$). Elevated amplitude difference between both wings is beneficial for stabilization of the visual target at high damping coefficients because of its large yaw moment equivalent. In WN-flies, FWHMs measured for 1024 pNms were thus similar to the values obtained from controls $(88.0 \pm 29.3°, N = 8)$. However, the kinematic benefit for object fixation behaviour at high damping is unfavourable for fixation precision at low damping because of frequent overshoots in feedback control. This also explains the early break-down of stripe control displayed by WN-flies (FWHM $> 90°$) at damping values below 520 pNms (figure 3c).

3.2. Optomotor altitude control

Figure 4a shows typical optomotor responses of tethered fruit flies, responding to a vertically oscillating horizontal stripe pattern presented under open-loop feedback conditions. This behavioural assay simulates unintended changes in flight altitude. Our data show that the tested flies respond to the vertical motion by symmetric and sinusoidal modulation of both the sum of left and right wingbeat amplitude, ΣWBA, and WBF, which results in a compensatory adjustment of aerodynamic lift. We found no significant difference of the mean top 1% maximum kinematic measures of each flight sequence between the tested groups $(p > 0.5$, figure 4$b,c)$, suggesting that sensory feedback from both halteres or wings is not necessary to maximize wing kinematics in fruit flies. However, we found a significant difference in the mean 1% minimum values between the groups. WN-flies consistently showed smaller minimum WBAs and frequencies in response to downward motion of the stripe grating than HI-flies and controls. Consequently, the kinematic envelope of total amplitude in WN-flies increases by 57% (amplitude range, $33.4 \pm 6.5°$, $N = 9, p = 0.03$), while the amplitude range of HI-flies decreases by 27% $(15.5 \pm 3.2°, N = 22, p = 0.04)$ compared with controls $(21.2 \pm 3.1°, N = 25,$ figure 4$d)$. We found similar trends in stroke frequency. While C-flies modulated stroke frequency by 23.3 ± 2.5 Hz, frequency modulation in HI-flies was 21.0 ± 1.5 Hz, which tends to be smaller $(p = 0.416)$, and modulation in WN-flies amounts to 38.5 ± 7.5 Hz, which is 66% larger $(p = 0.05)$ compared with controls.

3.3. Saccadic escape reflexes

Escape reflexes in *Drosophila* are vision-triggered fixed action motor patterns, allowing the animal to perform rapid, evasive manoeuvres to avoid obstacles and aerial predation [4,43]. Thus, precise control of wing motion during this motor sequence is of elevated ecological significance. One prominent reflex in flight of flies is the vision-triggered escape saccade, during which the fly rapidly turns its body between 90° and 180° within a few wing strokes [2,4,44]. We elicited saccadic turning by quickly expanding a black circular dot in the fly's lateral field of view, which mimics the approach of a dark object and robustly triggers saccadic responses [43]. To steer away from the lateral stimulus, tethered flies rapidly increase WBA on the ipsilateral and decrease amplitude on the contralateral body side (figure 5, top traces). These angular changes typically peak approximately 120 ms after stimulation onset, exhibiting mean ipsi- and contralateral amplitudes of $3.49 \pm 0.39°$ and $-2.36 \pm 0.43°$ (C-flies, $N = 24$),
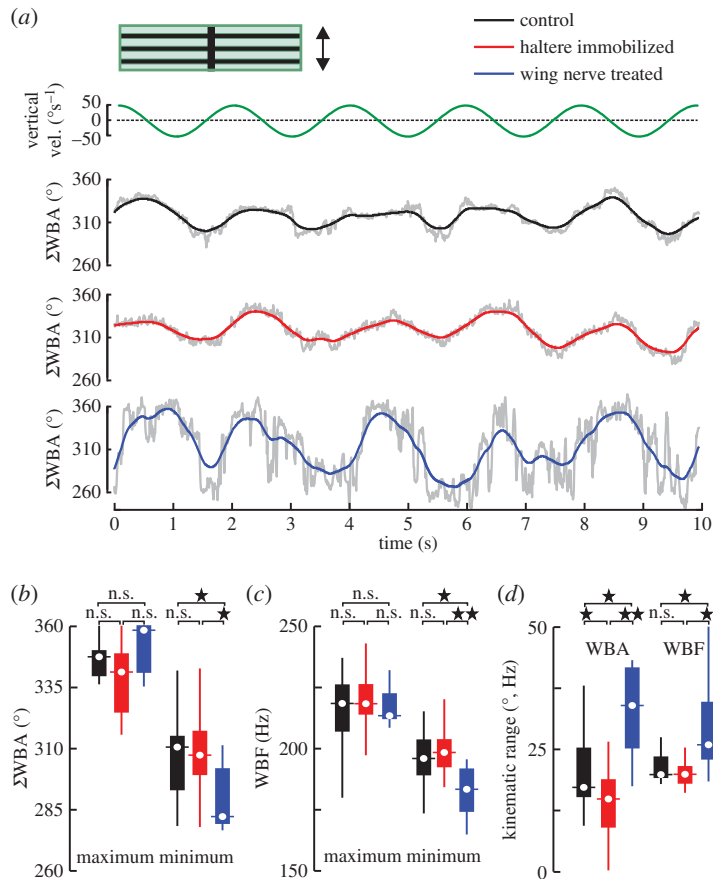
Figure 4. Optomotor lift response in tethered fruit flies. (*a*) Vertical velocity of horizontal stripe pattern (top) and sum of left and right wingbeat amplitude (ΣWBA, bottom) of single flies. Grey lines show raw data, coloured traces are low pass filtered and inset shows visual pattern. (*b–d*) Tukey box plots of top 1% maximum and 1% minimum (*b*) amplitude and (*c*) frequency (WBF) values of each flight sequence. (*d*) Kinematic range during lift response. See legends of figures 2 and 3 for more details.

respectively, relative to pre-saccadic kinematics. Consistent with the results in figure 3, WBAs of HI-flies were significantly reduced during the evasive response at 120 ms ($1.45 \pm 0.29°$, $p < 0.001$; $-1.34 \pm 0.32°$, $p = 0.002$; $N = 17$), while WN-flies showed elevated amplitudes ($6.46 \pm 1.67°$, $p < 0.001$; $-9.55 \pm 1.8°$ amplitude, $p = 0.03$; $N = 5$) of ipsi- and contralateral wings, respectively, compared with controls. To estimate yaw moment during the saccadic turning, we multiplied ΔWBA by the constant scaling factor 2.9×10^{-10} Nm deg^{-1} determined previously [41]. The results show that HI-flies produce approximately 50% smaller and WN-flies approximately 175% larger peak yaw moments than C-flies (figure 5, bottom traces; C-flies, 1.7 ± 0.19 nNm; HI-flies, 0.91 ± 0.33 nNm; WN-flies, 4.64 ± 0.65 nNm at 120 ms; $p < 0.001$ of all comparisons). Within the range of our temporal resolution (125 Hz sampling rate), we did not find significant differences in response delay (approx. 40 ms), time to peak response (approx. 190 ms) or response duration (approx. 1.5 s) due to the loss of sensory feedback. These values are consistent with previous measurements under similar conditions [43].

4. Discussion

This study investigated the significance of mechanosensory feedback signalling on visual steering performance of tethered flying fruit flies. The three behavioural assays—object fixation, altitude control and escape saccades—allowed us to study wing kinematics (amplitude, frequency) in response to dynamically changing visual stimuli. Neither the suppression of haltere feedback nor the attenuation of wing signalling completely repress vision-guided manoeuvring. Instead, we found a previously unknown antagonistic effect of these two proprioceptive inputs on visuomotor gain: haltere immobilization causes a decrease and wing nerve treatment an increase in wing steering range. A loss
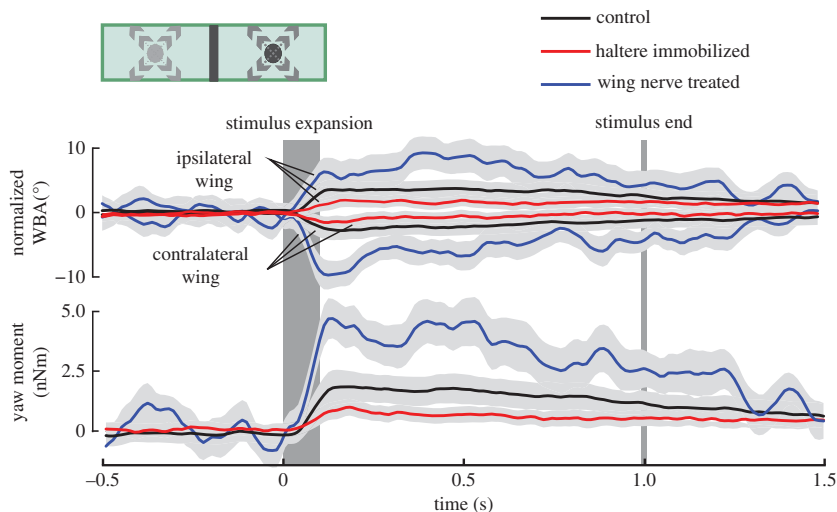
Figure 5. Wing kinematics and yaw moment during vision-triggered escape saccades. An expanding circular pattern is triggered at 0 s and expanded at a rate of 813° s^{-1} within 108 ms (dark grey). The pattern vanished 892 ms after stimulus onset from the panorama (grey line). Traces show mean responses of ipsi- (stimulus side) and contralateral wing that were offset-normalized by subtraction of mean pre-saccadic kinematics (top) and yaw moment (bottom). The plotted errors thus indicate the variance of relative wingbeat response. Before normalization, ipsilateral (contralateral) pre-saccadic amplitude was approximately $158 \pm 2.5°$ (approx. $158 \pm 2.2°$) in intact flies, approximately $152 \pm 2.6°$ (approx. $152 \pm 2.7°$) in haltere-immobilized flies and approximately $174 \pm 6.9°$ (approx. $176 \pm 7.3°$, means $\pm$ s.d.) in wing nerve treated flies. Ipsi- and lateral wing amplitude in both the HI-flies ($p = 0.40$) and wing-treated flies ($p = 0.34$) are not significantly different from that of controls. Light grey area around each data trace indicates one-fifth of the standard deviation. Black, intact controls ($N = 24$ flies, $n = 363$); red, haltere-immobilized flies ($N = 17$, $n = 246$); and blue, wing nerve treated flies ($N = 5$ flies, $n = 43$ trials).

of haltere feedback thus enhances object fixation performance while a loss of wing feedback reduces fixation performance under low aerodynamic damping conditions.

4.1. Vision-guided flight in tethered animals

Behavioural experiments in flies that involve manipulations of sensory pathways can often only be conducted under tethered flight conditions, owing to the loss of body stability in free flight. Immobilization of the halteres reduces the gyroscopic feedback that is known to be essential for stable free flight. The same holds for wing nerve signalling because flies experiencing bilateral laser treatment of wing nerves with 35 mW lose their ability to manoeuvre freely. Tethering is thus a necessity in our investigation but hinders the animal to physically move its body during turning manoeuvres. The loss of gyroscopic feedback from the halteres due to tethering probably puts tethered flying flies into a state of sensory conflict as described in detail by Taylor *et al.* [45]. Haltere immobilization might reduce this sensory conflict as it prevents the generation of ambiguous residual signalling. Despite these constraints, the tethered flight paradigm has been proved a powerful tool, especially for the investigation of visual flight control mechanisms [46].

4.2. Direct visual input to wing steering muscles

Consistent with the results of Mureli & Fox [32], our results show that flies with disabled halteres may cope with visual steering tasks, rejecting an exclusive re-routing of visual feedback through the haltere system. It is thus likely that the neural pathway from the visual system to WSM circumvents the haltere's mechanoreceptors. This view is also supported by previous anatomical and physiological studies on neurons controlling thoracic neck muscles, indirect flight power muscles, and WSM in flies. Intracellular recordings combined with dye filling show that in Diptera, more than 50 pairs of visual motion-sensitive descending neurons from the brain terminate bilaterally in superficial pterothoracic neuropils at the level of power muscle motor neurons [47]. Other motion-sensitive descending neurons that respond to yaw, pitch and roll movements of the fly provide segmental collaterals to neuropils containing WSM and neck-muscle motor neurons [47]. A study on male flesh flies further showed that descending visual

interneurons are dye-coupled to motoneurons of the two most prominent steering muscles, b1 and b2 [48]. The apparent absence of vision-evoked electrical responses in WSM that has been reported by Chan *et al.* [30] in *Calliphora* might reflect a gating process in their quiescent preparation. This view is supported by electrophysiological studies on visual interneurons and neck muscles of flies. The studies highlight that visual stimulation only induces spiking of neck-muscle motoneurons during locomotor activity [33], which leads to an increase in gain of visual interneurons [49,50], or does require additional stimulation of mechanoreceptors [51].

A direct visual pathway from the brain to the WSM in flies raises the question of how the comparably slow, non-phasic signals from the visual system are integrated into the rapid, phase-coded motor system [18]. Motoneurons of WSM usually generate no more than a single spike within the approximately 5 ms wing stroke cycle of fruit flies. Muscle spike frequencies above stroke frequency are rare events and limited to extreme cases such as take-off behaviour in fruit flies [52]. Thus, flies may control WSM tension only by bulk activation of muscle fibres or by changes in timing of muscle spikes relative to the wing stroke cycle. It has previously been shown that muscle spike activation phase determines WSM power output and efficacy by which WSM alter wing kinematics [52–55]. As even subtle kinematic modulations result in comparably large changes in aerodynamic force production [56], a precise timing of muscle activation within a few milliseconds time window is crucial for successful manoeuvring and stable flight in flies [57]. The output of the visual system may not provide phase-locked signals in real time because of the relatively long time that is required for photo-transduction, visual motion sensing and processing of at least approximately 6 ms using feedback from the ocelli [58] and approximately 30 ms from the compound eyes [59]. In this context, the exact function of projections from mechanoreceptors of wings and halteres that converge on visual circuits upstream in the suboesophageal ganglion is not well understood [60].

A physiological mechanism for integration of non-phasic visual information and phasic proprioceptive feedback arises from recent observations on graded, non-spiking responses of visual interneurons [61] and sustained, subthreshold depolarization of neck motoneurons following visual stimulation in flies [51]. According to these findings, we here propose that visual input to WSM motoneurons leads to sustained changes in membrane potential that remain subthreshold. This subthreshold potential and feedback from mechanoreceptors on wings and the halteres are then integrated by the motoneuron throughout the wing stroke cycle. Consequently, the relative timing of WSM spike generation by its motoneuron relies on the membrane potential provided by the graded visual input. This idea is based on the assumption that spike initiation owing to phasic, synaptic input from proprioceptors is probably delayed in a hyperpolarized membrane owing to the time required for depolarization above threshold. The campaniform sensillae of wings and halteres provide long-lasting volleys of phase-locked action potentials [17,18] owing to different latencies of the sensory cells to mechanical stimuli [20]. In crane flies, Fox & Daniel [20] reported values ranging from approximately 2.2 to approximately 15.9 ms delay of the approximately 25 ms wing stroke period. If timing of spike initiation in WSM motoneurons is due to postsynaptic integration of consecutive potentials, any shift in vision-induced membrane potential is probably converted into a change in spiking phase relative to the stroke cycle. In this sense, proprioceptive feedback provides a preferred phase for muscle activation that is adjusted by the visual system, which is consistent with the finding that visual feedback modulates the firing phase of WSM in fruit flies [55].

4.3. Proprioceptive control of visuomotor gain

Our study shows a previously unknown opposing influence of mechanosensory feedback on vision-guided behaviour in flies (figure 3). In haltere-immobilized animals, we observed a decrease in WBA steering range together with an increase in fixation performance during low damping conditions. While the decrease in steering range following haltere immobilization might imply that visual steering commands are at least partially rerouted through the haltere system, this interpretation does not explain why the steering range increases in wing nerve treated animals. An antagonistic effect on amplitude control is particularly puzzling because afferent nerves of both wings and halteres provide excitatory input to WSM motoneurons [22].

A possible explanation for the—at the first sight paradoxical—antagonistic influence of the two excitatory inputs resides in the nonlinear, biomechanical properties of WSM. Previous work on the relationship between muscle activation phase and muscle work in the prominent basalare WSM b1 and b2 showed that mechanical muscle work output changes approximately sinusoidally with increasing activation phase [52,54]. Incorporating these biomechanical properties of WSM into the control
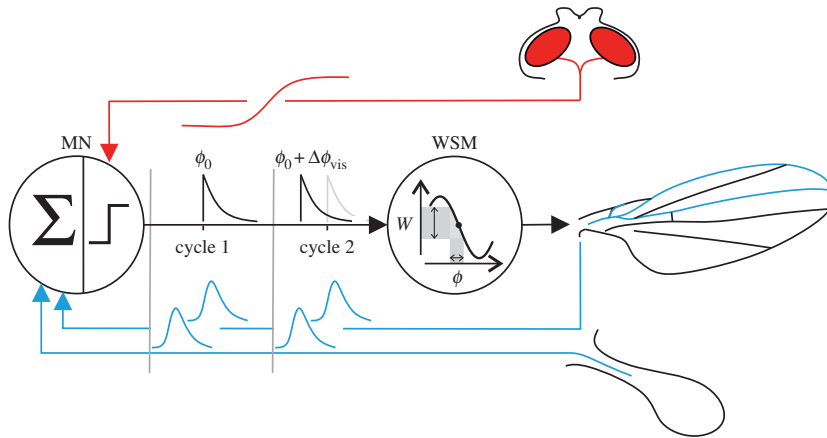
Figure 6. Feedback control loop for flight. Phasic mechanosensory feedback signals are integrated by the muscle motoneuron (MN), providing a set-point for wing steering muscle (WSM) activation on the muscle's nonlinear phase-efficacy curve. Graded visual input alters the firing threshold of the motoneuron, which turns into an temporal advance in spike phase with respect to the stroke cycle (cycle 2). Changes in spiking phase are thought to cause changes in effective muscle work (*W*) and consequently changes in wing kinematics.

circuitry leads to a more comprehensive hypothetical model for wing control in flies that explains our contradictory findings (figure 6). Assuming that proprioceptive feedback provides a preferred muscle activation phase, ϕ_0, and the visual system adjusts this phase by $\Delta\phi_{\text{vis}}$, the effective change in muscle work, ΔW, owing to phase shift is given by

$$\Delta W_{\phi_0} = W(\phi_0 + \Delta\phi_{\text{vis}}) - W(\phi_0). \qquad (4.1)$$

The change of WSM work thereby depends on the slope of the work response curve near activation phase ϕ_0. Based on this consideration and the intriguing study by Sponberg & Daniel [62] on phase control of moth flight muscles, we may derive the gain of visuomotor work phase, G_0, from the equation

$$G_0 = \Delta W_{\phi_0} \Delta\phi_{\text{vis}}^{-1}. \qquad (4.2)$$

This framework allows us to attribute our behavioural findings to changes in phase-dependent local slopes of muscle work output and thus to the link between muscle mechanics and neural phasing. WMS in flies have dedicated preferred activation phases and thus different phase-dependent local work response slopes [18,25,52,55]. For example, during unperturbed flight in fruit flies, the preferred activation phase of the basalare muscle b2 is approximately 0.20 stroke cycle [52,55], at which the corresponding local muscle efficacy and muscle response slope is intermediate [52]. If ablation of wing feedback signalling shifts the preferred phase to a steeper part of the nonlinear response curve, any phase adjustment by the visual system results in an increase in visuomotor gain, and thus vision-controlled increase in modulation of WBAs. As in this case temporal phase errors owing to intrinsic noise are also amplified, an increase in visuomotor gain is consistent with the observed decrease in fixation performance as shown in figure 2. The opposing effect of haltere immobilization on steering range and fixation performance is likewise explained by a smaller visuomotor gain, resulting from a shift of the preferred phase to a less steep part of the nonlinear response curve. At small damping, subtle modulation in wing kinematics is sufficient to stabilize the stripe in the animal's frontal field of view, while elevated kinematic modulation frequently causes a heading destabilization towards the visual target. The decrease in phase error that comes along with the decrease in visuomotor gain in HI-flies is thus beneficial for fixation performance at low damping coefficients.

A possible reason why the two excitatory inputs to WSM motoneurons cause different phase shifts might be because of their different excitatory postsynaptic components [22]. In blowflies, these synaptic differences suggest that the two sensory pathways have different strength to evoke postsynaptic action potentials in WSM motoneurons. Compared with the haltere feedback, the wing pathway is apparently stronger to entrain the motoneuron over a wide range of muscle activation phases [22]. The emergence of gain modulation on the behavioural level suggests that the two proprioceptive modalities are finely balanced with the biomechanical properties of WSM and the computational properties of the WSM motoneurons. During free flight, flies perform a wide variety of manoeuvres and are frequently subject to turbulent air flows. Haltere feedback is modulated by Coriolis forces caused by body rotations, and wing mechanoreceptors respond to changes in aerodynamic and inertial forces acting locally on the wing

during flapping [3,28,57]. The preferred phase for muscle activation and, consequently, the instantaneous WSM work-phase gain, thus probably varies in each wing stroke depending on the animal's current locomotor state and environment.

5. Conclusion

Motor control systems in vertebrates and invertebrates share several common principles. For guided locomotion, most animals use both continuous feedback provided by directional senses such as vision, olfaction and hearing, and phasic proprioceptive feedback from mechanoreceptors modulating motor activity on a cycle-by-cycle basis [1]. These sensory inputs are often integrated by central pattern generators, specialized neural circuitries that generate the neural rhythm needed for periodic muscle activation [63]. In Diptera, the central pattern generator that determines the locomotor cycle is replaced by a mechanical, thoracic oscillator that is driven by the power of myogenic, asynchronous flight muscles [12,18,24,64,65]. In these animals, sensory input for flight control converges on the level of steering muscle motoneurons [22,31,32]. The sensory integration in flies thus conceptually represents a *local sensory feedback* circuitry that has also been found in stick insects [66], cats [67] and humans [68]. In such simplified feedback loops, the connections from sensory neurons bypass the central pattern generator and directly alter spiking probability of motoneurons within milliseconds [69]. Assuming that the dynamic regulation of visuomotor gain by proprioceptive feedback controls muscle spiking phase, this process might lead to a behaviour with optimal trade-off between flight stability and agility in *Drosophila*. Consequently, the specialized *local sensory feedback* loop may provide the substrate of the elevated aerial performance and is thus a prerequisite for the biological fitness of this animal.

References

1. Dickinson MH, Farley CT, Full RJ, Koehl MA, Kram R, Lehman S. 2000 How animals move: an integrative view. *Science* **288**, 100–106. (doi:10.1126/science.288.5463.100)

2. Fry SN, Sayaman R, Dickinson MH. 2003 The aerodynamics of free-flight maneuvers in *Drosophila*. *Science* **300**, 495–498. (doi:10.1126/science.1081944)

3. Dickinson MH. 2005 The initiation and control of rapid flight maneuvers in fruit flies. *Integr. Comp. Biol.* **45**, 274–281. (doi:10.1093/icb/45.2.274)

4. Muijres FT, Elzinga MJ, Melis JM, Dickinson MH. 2014 Flies evade looming targets by executing rapid visually directed banked turns. *Science* **344**, 172–177. (doi:10.1126/science.1248955)

5. Borst A, Egelhaaf M. 1989 Principles of visual motion detection. *Trends Neurosci.* **12**, 297–306. (doi:10.1016/0166-2236(89)90010-6)

6. Mayer M, Vogtmann K, Bausenwein B, Wolf R, Heisenberg M. 1988 Flight control during 'free yaw turns' in *Drosophila melanogaster*. *J. Comp. Physiol.* **163**, 389–399. (doi:10.1007/BF00604014)

7. Bender JA, Dickinson MH. 2006 Visual stimulation of saccades in magnetically tethered *Drosophila*. *J. Exp. Biol.* **209**, 3170–3182. (doi:10.1242/jeb.02369)

8. Fraenkel G, Pringle JWS. 1938 Halteres of flies as gyroscopic organs of equilibrium. *Nature* **141**, 919–920. (doi:10.1038/141919a0)

9. Faust R, Buddenbrock W. 1951 Die Regulierung des Gleichgewichtes der höheren Dipteren durch die Halteren. *Experientia* **7**, 265–266. (doi:10.1007/BF02154545)

10. Sandeman DC. 1980 Angular acceleration, compensatory head movements and the halteres of flies (*Lucilia serricata*). *J. Comp. Physiol. A* **136**, 361–367. (doi:10.1007/BF00657358)

11. Ristroph L, Bergou AJ, Ristroph G, Coumes K, Berman GJ, Guckenheimer J, Wang ZJ, Cohen I. 2010 Discovering the flight autostabilizer of fruit flies by inducing aerial stumbles. *Proc. Natl Acad. Sci. USA* **107**, 4820–4824. (doi:10.1073/pnas.1000615107)

12. Bartussek J, Mutlu AK, Zapotocky M, Fry SN. 2013 Limit-cycle-based control of the myogenic wingbeat rhythm in the fruit fly *Drosophila*. *J. R. Soc. Interface* **10**, 20121013. (doi:10.1098/rsif.2012.1013)

13. Gnatzy W, Grünert U, Bender M. 1987 Campaniform sensilla of *Calliphora vicina* (Insecta, Diptera). *Zoomorphology* **106**, 312–319. (doi:10.1007/BF00312005)

14. Fayyazuddin A, Dickinson MH. 1996 Haltere afferents provide direct, electrotonic input to a steering motor neuron in the blowfly, *Calliphora*. *J. Neurosci.* **16**, 5225–5232.

15. Dickinson MH, Tu MS. 1997 The function of dipteran flight muscle. *Comp. Biochem. Phys. A* **116**, 223–238. (doi:10.1016/S0300-9629(96)00162-4)

16. Cole ES, Palka J. 1982 The pattern of campaniform sensilla on the wing and haltere of *Drosophila melanogaster* and several of its homeotic mutants. *J. Embryol. Exp. Morph.* **71**, 41–61.

17. Pringle JWS. 1948 The gyroscopic mechanism of the halteres of Diptera. *Phil. Trans. R. Soc. Lond. B* **233**, 347–384. (doi:10.1098/rstb.1948.0007)

18. Heide G. 1983 Neural mechanisms of flight control in diptera. In *BIONA—report 2* (ed. W Nachtigall), pp. 35–52. Stuttgart, Germany: G. Fischer. Akad. Wiss. Mainz.

19. Nalbach G. 1993 The halteres of the blowfly *Calliphora*. I. Kinematics and dynamics. *J. Comp. Physiol. A* **173**, 293–300. (doi:10.1007/BF00212693)

20. Fox JL, Daniel TL. 2008 A neural basis for gyroscopic force measurement in the halteres of Holorusia. *J. Comp. Physiol. A* **194**, 887–897. (doi:10.1007/s00359-008-0361-z)

21. Fox JL, Fairhall AL, Daniel TL. 2010 Encoding properties of haltere neurons enable motion feature detection in a biological gyroscope. *Proc. Natl Acad. Sci. USA* **107**, 3840–3845. (doi:10.1073/pnas.0912548107)

22. Fayyazuddin A, Dickinson MH. 1999 Convergent mechanosensory input structures the firing phase of a steering motor neuron in the blowfly, *Calliphora*. *J. Neurophysiol.* **82**, 1916–1926.

23. Dickerson BH, Aldworth ZN, Daniel TL. 2014 Control of moth flight posture is mediated by wing mechanosensory feedback. *J. Exp. Biol.* **217**, 2301–2308. (doi:10.1242/jeb.103770)

24. Heide G. 1979 Proprioceptive feedback dominates the central oscillator in the patterning of the flight motoneuron output in Tipula (Diptera). *J. Comp. Physiol. A* **134**, 177–189. (doi:10.1007/BF00610477)

25. Balint CN, Dickinson MH. 2001 The correlation between wing kinematics and steering muscle activity in the blowfly *Calliphora vicina*. *J. Exp. Biol.* **204**, 4213–4226.

26. Hengstenberg R. 1991 Stabilizing head movements in the blowfly *Calliphora*. *Zool. Jahrb. Allg. Zool.* **95**, 297–304.

27. Dickinson MH. 1990 Comparison of encoding properties of campaniform sensilla on the fly wing. *J. Exp. Biol.* **151**, 245–261.

28. Taylor GK, Krapp HG. 2007 Sensory systems and flight stability: what do insects measure and why? In *Insect mechanics and control* (eds J Casas, SJ Simpson), pp. 231–316. New York, NY: Academic Press.

29. Frye MA. 2010 Multisensory systems integration for high-performance motor control in flies. *Curr. Opin. Neurobiol.* **20**, 347–352. (doi:10.1016/j.conb.2010.02.002)

30. Chan WP, Prete F, Dickinson MH. 1998 Visual input to the efferent control system of a fly's 'gyroscope'. *Science* **280**, 289–292. (doi:10.1126/science.280.5361.289)

31. Sherman A, Dickinson MH. 2004 Summation of visual and mechanosensory feedback in *Drosophila* flight control. *J. Exp. Biol.* **207**, 133–142. (doi:10.1242/jeb.00731)

32. Mureli S, Fox JL. 2015 Haltere mechanosensory influence on tethered flight behavior in *Drosophila*. *J. Exp. Biol.* **218**, 2528–2537. (doi:10.1242/jeb.121863)

33. Haag J, Wertz A, Borst A. 2010 Central gating of fly optomotor response. *Proc. Natl Acad. Sci. USA* **107**, 20 104–20 109. (doi:10.1073/pnas.1009381107)

34. Fang Y, Soares L, Bonini NM. 2013 Design and implementation of *in vivo* imaging of neural injury responses in the adult *Drosophila* wing. *Nat. Protocols* **8**, 810–819. (doi:10.1038/nprot.2013.042)

35. Sinha S, Liang L, Ho ETW, Urbanek KE, Luo L, Baer TM, Schnitzer MJ. 2013 High-speed laser microsurgery of alert fruit flies for fluorescence imaging of neural activity. *Proc. Natl Acad. Sci. USA* **110**, 18 374–18 379. (doi:10.1073/pnas.1216287110)

36. Lin Y, Wu M, Hsiao P, Chu L, Yang M, Fu C, Chiang A. 2015 Three-wavelength light control of freely moving *Drosophila melanogaster* for less perturbation and efficient social-behavioral studies. *Biomed. Opt. Express* **6**, 514–523. (doi:10.1364/BOE.6.000514)

37. Yoon J, Ryu S-W, Lee S, Choi C. 2015 Cytosolic irradiation of femtosecond laser induces mitochondria-dependent apoptosis-like cell death via intrinsic reactive oxygen cascades. *Sci. Rep.* **5**, 8231. (doi:10.1038/srep08231)

38. Deora T, Singh AK, Sane SP. 2015 Biomechanical basis of wing and haltere coordination in flies. *Proc. Natl Acad. Sci. USA* **112**, 1481–1486. (doi:10.1073/pnas.1412279112)

39. Lehmann FO, Dickinson MH. 1998 The control of wing kinematics and flight forces in fruit flies (*Drosophila* spp.). *J. Exp. Biol.* **201**, 385–401.

40. Götz KG. 1968 Flight control in *Drosophila* by visual perception of motion. *Kybernetik* **4**, 199–208. (doi:10.1007/BF00272517)

41. Hesselberg T, Lehmann F-O. 2007 Turning behaviour depends on frictional damping in the fruit fly *Drosophila*. *J. Exp. Biol.* **210**, 4319–4334. (doi:10.1242/jeb.010389)

42. Lehmann F-O. 2010 The limits of turning control in flying insects. In *Flying insects and robots* (eds D Floreano, J-C Zufferey, MV Srinivasan, C Ellington), pp. 231–246. Berlin, Germany: Springer.

43. Tammero LF, Dickinson MH. 2002 Collision-avoidance and landing responses are mediated by separate pathways in the fruit fly, *Drosophila melanogaster*. *J. Exp. Biol.* **205**, 2785–2798.

44. Mronz M, Lehmann F-O. 2008 The free-flight response of *Drosophila* to motion of the visual environment. *J. Exp. Biol.* **211**, 2026–2045. (doi:10.1242/jeb.008268)

45. Taylor GK, Bacic M, Bomphrey RJ, Carruthers AC, Gillies J, Walker SM, Thomas ALR. 2008 New experimental approaches to the biology of flight control systems. *J. Exp. Biol.* **211**, 258–266. (doi:10.1242/jeb.012625)

46. Borst A. 2014 Fly visual course control: behaviour, algorithms and circuits. *Nat. Rev. Neurosci.* **15**, 590–599. (doi:10.1038/nrn3799)

47. Strausfeld NJ, Gronenberg W. 1990 Descending neurons supplying the neck and flight motor of Diptera: organization and neuroanatomical relationships with visual pathways. *J. Comp. Neurol.* **302**, 954–972. (doi:10.1002/cne.903020419)

48. Gronenberg W, Strausfeld NJ. 1991 Descending pathways connecting the male-specific visual system of flies to the neck and flight motor. *J. Comp. Physiol. A* **169**, 413–426. (doi:10.1007/BF00197654)

49. Maimon G, Straw AD, Dickinson MH. 2010 Active flight increases the gain of visual motion processing in *Drosophila*. *Nat. Neurosci.* **13**, 393–399. (doi:10.1038/nn.2492)

50. Rosner R, Egelhaaf M, Warzecha AK. 2010 Behavioural state affects motion-sensitive neurones in the fly visual system. *J. Exp. Biol.* **213**, 331–338. (doi:10.1242/jeb.035386)

51. Huston SJ, Krapp HG. 2009 Nonlinear integration of visual and haltere inputs in fly neck motor neurons. *J. Neurosci.* **29**, 13 097–13 105. (doi:10.1523/JNEUROSCI.2915-09.2009)

52. Lehmann F-O, Götz KG. 1996 Activation phase ensures kinematic efficacy in flight-steering muscles of *Drosophila melanogaster*. *J. Comp. Physiol.* **179**, 311–322. (doi:10.1007/BF00194985)

53. Tu MS, Dickinson MH. 1996 The control of wing kinematics by two steering muscles of the blowfly (*Calliphora vicina*). *J. Comp. Physiol. A* **178**, 813–830. (doi:10.1007/BF00225830)

54. Tu MS, Dickinson MH. 1994 Modulation of negative work output from a steering muscle of the blowfly *Calliphora vicina*. *J. Exp. Biol.* **192**, 207–224.

55. Heide G, Götz KG. 1996 Optomotor control of course and altitude in *Drosophila melanogaster* is correlated with distinct activities of at least three pairs of flight steering muscles. *J. Exp. Biol.* **199**, 1711–1726.

56. Sane SP, Dickinson MH. 2001 The control of flight force by a flapping wing: lift and drag production. *J. Exp. Biol.* **204**, 2607–2626.

57. Dickinson MH. 2006 Insect flight. *Curr. Biol.* **16**, R309–R314. (doi:10.1016/j.cub.2006.03.087)

58. Parsons MM, Krapp HG, Laughlin SB. 2010 Sensor fusion in identified visual interneurons. *Curr. Biol.* **20**, 624–628. (doi:10.1016/j.cub.2010.01.064)

59. Hardie CR, Raghu P. 2001 Visual transduction in *Drosophila*. *Nature* **413**, 186–193. (doi:10.1038/35093002)

60. Chan WP, Dickinson MH. 1996 Position-specific central projections of mechanosensory neurons on the haltere of the blow fly, *Calliphora vicinam*. *J. Comp. Neurol.* **369**, 405–418. (doi:10.1002/(SICI)1096-9861(19960603))

61. Haag J, Wertz A, Borst A. 2007 Integration of lobula plate output signals by DNOVS1, an identified premotor descending neuron. *J. Neurosci.* **27**, 1992–2000. (doi:10.1523/JNEUROSCI.4393-06.2007)

62. Sponberg S, Daniel TL. 2012 Abdicating power for control: a precision timing strategy to modulate function of flight power muscles. *Proc. R. Soc. B.* **279**, 3958–3966. (doi:10.1098/rspb2012.1085)

63. Ijspeert AJ. 2008 Central pattern generators for locomotion control in animals and robots: a review. *Neural Netw.* **21**, 642–653. (doi:10.1016/j.neunet.2008.03.014)

64. Pringle JWS. 1949 The excitation and contraction of the flight muscles of insects. *J. Physiol.* **108**, 226–232. (doi:10.1113/jphysiol.1949.sp004326)

65. Danzer A. 1956 Der Flugapparat der Dipteren als Resonanzsystem. *Z. vgl. Physiol.* **38**, 259–283. (doi:10.1007/BF00341301)

66. Büschges A, Gruhn M. 2007 Mechanosensory feedback in walking: from joint control to locomotor patterns. In *Advances in insect physiology*, vol. 34 (eds J Casas, SJ Simpson), pp. 193–230. New York, NY: Academic Press.

67. Ekeberg Ö, Pearson KG. 2005 Computer simulation of stepping in the hind legs of the cat: an examination of mechanisms regulating the stance-to-swing transition. *J. Neurophysiol.* **94**, 4256–4268. (doi:10.1152/jn.00065.2005)

68. Yang JF, Gorassini M. 2006 Spinal and brain control of human walking: implications for retraining of walking. *Neuroscientist*, **12**, 379–389. (doi:10.1177/1073858406292151)

69. Büschge A, Scholz H, El Manira A. 2011 New moves in motor control. *Curr. Biol.*, **21**, 513–524. (doi:10.1016/j.cub.2011.05.029)